Manuscript for *Revista Mexicana de Astronomía y Astrofísica* (2007)

RADIAL ABUNDANCE GRADIENTS FROM PLANETARY NEBULAE AT DIFFERENT DISTANCES FROM THE GALACTIC PLANE

W. J. Maciel,[1] R. D. D. Costa,[1] and O. Cavichia[2]

Draft version: May 29, 2015

RESUMEN

ABSTRACT

We investigate the variations of the radial O/H abundance gradients from planetary nebulae (PN) located at different distances from the galactic plane. In particular, we determine the abundance gradients at different heights from the plane in order to investigate a possible gradient inversion for the objects at larger distances from the plane. We consider a large sample of PN with known distances, so that the height relative to the galactic plane can be derived, and accurate abundances, so that the gradients can be determined.

Key Words: Galaxies: Abundances — Galaxies: Disk — ISM: abundances — ISM: planetary nebulae: general

1. INTRODUCTION

There are some evidences that the galactic radial abundance gradient from elements such as Fe, O, etc. changes according to the ages of the objects considered. Two main modifications have been suggested in the literature: first, the average abundances decrease as older objects are considered, and the gradient itself may or may not be affected. Second, there are some suggestions that in older objects there is an inversion of the gradients at low galactocentric distances, $R < 8\,\mathrm{kpc}$, approximately, in the sense that the decreasing outwards abundances also decrease inwards, as older objects are considered (see for example Sancho-Miranda et al. 2014, Cheng et al. 2012a, 2012b, Carrell et al. 2012).

The results by Cheng et al. (2012a, 2012b) suggest that the radial gradients flatten out at large distances from the plane, which is confirmed by a sample of dwarf stars from the SEGUE survey at $7 < R(\mathrm{kpc}) < 10.5$ with proper motions and spectroscopic abundances by Carrell et al. (2012). The latter includes objects up to $|z| \simeq 3\,\mathrm{kpc}$, for which slightly positive gradient are obtained for the [Fe/H] ratio. Other previous investigations for thick disk stars also led to flat or slightly positive gradients (Allende-Prieto et al. 2006, Nordström et al. 2004).

Some recent chemical evolution models predict a strong flattening of the [Fe/H] radial gradient for higher distances from the galactic plane, $|z| >$

[1]Instituto de Astronomia, Geofísica e Ciências Atmosféricas, Universidade de São Paulo, Brazil.

[2]Instituto de Física e Química, Universidade Federal de Itajubá, Brazil.

0.5 kpc, as shown for example by Minchev et al. (2014, see also Chiappini et al. 2015 and references therein). These models take into account radial migration, and suggest an inversion of the gradient, from negative to weakly positive, for $R < 10$ kpc and $0.5 < |z| < 1.0$ kpc. Also, theoretical models by Curir et al. (2012) and Spitoni & Matteucci (2011) predict a gradient inversion at galactocentric distances of about 10 kpc for the early Galaxy (about 2 Gyr), which is a consequence of the inside-out formation of the thick disk.

Differences in the radial abundance gradients are also supported by Fe/H and Si/H gradients as derived for red clump stars from the RAVE survey, in the sense that the steeper gradients occur for low distances to the plane, becoming flatter for higher z values. A slightly positive gradient has been found from APOGEE data for stars at $1.5 < z(\mathrm{kpc}) < 3.0$ (Chiappini et al. 2015, Boeche et al. 2014).

Planetary nebulae may give some contribution to this problem. The nebulae in the disk of the Galaxy are spread along at least 1 kpc above (or below) the galactic plane, that is, these objects have typically $0 < |z|(\mathrm{pc}) < 1,000$. In view of the number of PN with known abundances, which is of the order of about 300 objects, it is possible that considering objects at different heights from the plane, some differences between the derived gradients may be determined. In principle, PN located higher from the galactic plane are produced by older stars, as in the case of the halo PN, which are very probably older than the disk nebulae.

In this work, we investigate the possible variations in the radial abundance gradients when objects at different distances from the galactic plane are taken into account. We examine a large sample of galactic PN with known distances and accurate abundances, so that both the height z relative to the galactic plane and the galactocentric distance R can be determined, apart from the radial abundance gradients. We consider the oxygen abundance ratio O/H, which has been derived for a large number of objects and present the smallest uncertainties in the abundances.

2. THE DATA

The main problem in studying gradients from planetary nebulae is to obtain their distances. In this paper, we will consider the objects from the Magellanic Cloud calibration by Stanghellini et al. (2008) and, in particular from Stanghellini and Haywood (2010, hereafter SH), who also give chemical abundances. This is the most recent sizable distance scale in the literature, so that the probability of obtaining a reasonable estimate of the gradients is higher. Table 1 of Stanghellini and Haywood (2010) includes 728 objects, which will be our starting sample. The objects are referenced by their PNG number, to which we added the common names from the catalogue by Acker et al. (1992). Table 2 of Stanghellini and Haywood (2010) gives nebular abundances of He, N, O, and Ne for a smaller sample, containing 224 objects. Since the galactic coordinates (l, b) are known, by taking the distances into account, the z coordinate can be obtained, as well as the galactocentric distance

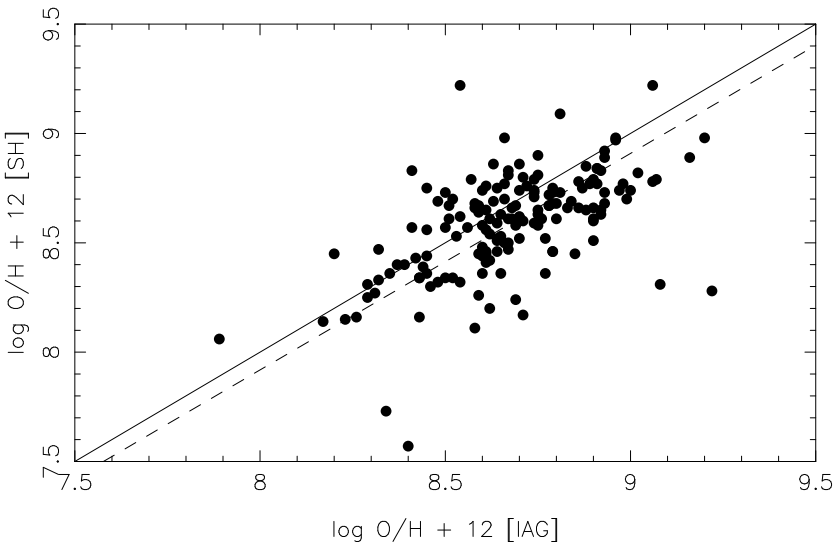

Fig. 1. Comparison of the oxygen abundances by Stanghellini & Haywood (2010) (y axis) and the abundances by the IAG sample (x axis).

R, adopting $R_0 = 8\,\mathrm{kpc}$ for the distance of the Sun to the galactic centre. As an alternative to the abundances given by SH, we will also consider the abundances by the IAG group as discussed for example by Maciel and Costa (2013). This includes 234 disk nebulae. Considering the objects of both samples as part of the 728 PN sample given by SH, oxygen abundances are known for 201 objects from the SH sample; 222 objects from the IAG sample; 160 objects in common for the SH and IAG samples, and 263 objects including all objects with abundances in at least one of the two samples. This is the initial sample of galactic disk planetary nebulae that we will consider in this paper.

The reason why we can safely consider both samples (SH and IAG) concerning their oxygen chemical abundances can be seen in Figure 1, where we plot the SH oxygen abundances (y axis) as a function of the IAG abundances (x axis). A linear fit of the form $y = a\,x$ gives the following results: $a = 0.9898$, with a standard deviation $\sigma = 0.0019$, and correlation coefficient $r = 0.9997$, with an uncertainty $\sigma_r = 0.2096$. The least squares fit line (dashed line) is very close to the one-to-one line (full line), only slightly displaced downwards by about 0.05 dex. It can be seen that only a few nebulae have higher deviations than the average.

3. THE METHOD

In order to investigate the possible variations of the abundance gradient for older objects, which are in principle located higher above the galactic plane, we have divided the 263 object sample into several groups, according to the z values, which were then compared with the results for the whole sample. Once the groups have been defined, the procedure consists in plotting

$\epsilon(\mathrm{O}) = \log \mathrm{O/H} + 12$ as a function of the galactocentric distance R, and estimating the average linear gradient, as defined by the equation

$$\epsilon(\mathrm{O}) = \log \mathrm{O/H} + 12 = A + B\ R \tag{1}$$

and then estimating the coefficients A and B, their uncertainties and the correlation coefficient r. Alternatively, we are also interested in investigating any possible variation of the slope B along the galactocentric radius, so that we will also obtain polynomial fits using a second degree function defined as

$$\epsilon(\mathrm{O}) = C + D\ R + E\ R^2 \tag{2}$$

and then estimating the coefficients C, D, E, and the χ square value. We have considered two cases: Case A, in which we have adopted the abundances by SH if both samples present abundances for the same object, and Case B, in which abundances from the IAG sample were selected in this case. As it turned out, both Case A and B produce essentially the same results, so that most figures presented here are for Case A.

4. RESULTS AND DISCUSSION

4.1. *The Total Disk Sample*

The first results are obtained for the whole sample of 263 objects, both for Case A and B. The derived linear fits defined as in equation (1) are shown in the first two lines of Table 1. The corresponding figures are shown in Figure 2, which extends up to 15 kpc from the centre, so that the few objects at higher galactocentric distances are not included. It can be seen that in both cases an average gradient $d(\mathrm{O/H})/dR \simeq -0.02$ to -0.03 dex/kpc is obtained. The average uncertainty in the abundances are about -0.2 dex. The dispersion is larger at larger galactocentric distances, as expected, and the correlation coefficient is relatively low, which is a consequence of the relatively flat gradient and the uncertainties in the abundances.

We can probably get a more meaningful result by dividing the sample according to their galactocentric distances, for example using 2 kpc bins. We have considered 9 bins, and the results are shown in Figure 3, where the data points are shown as empty circles and the average abundances in each bin as filled circles. The vertical error bars show the mean deviation and the horizontal bars show the adopted galactocentric limits. The dashed line shows the linear fits as given by lines 3 and 4 of Table 1.

A comparison of the dashed lines in figures 2 and 3 show that they are very similar, that is, the linear fits of the whole sample and of the binned data are essentially the same. This can also be seen from Table 1, which shows that the intercept and slope of both lines are very similar. However, the correlation coefficients of the binned data are much higher than for the whole sample.

A more detailed analysis can be made obtaining a polynomial fit to the data, so that any slope variation with position can be estimated. We have

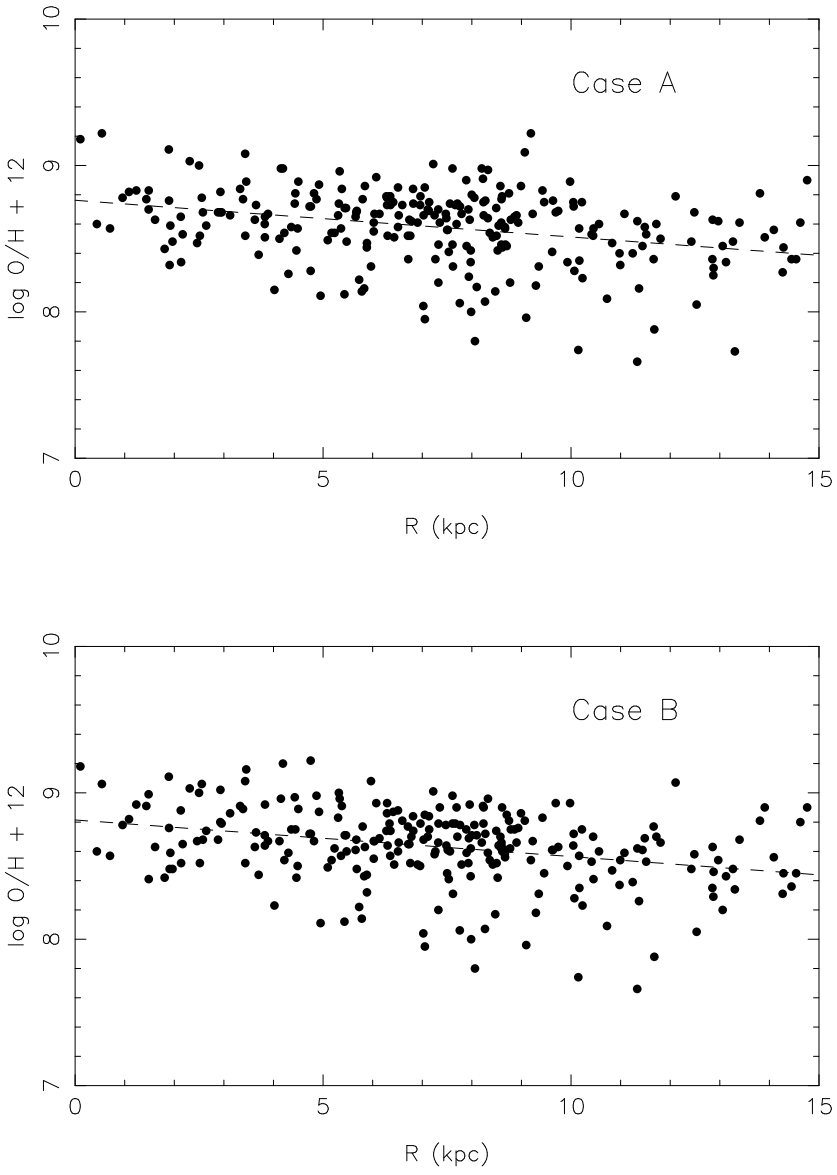

Fig. 2. Variation of the oxygen abundance with the galactocentric distance for the whole sample, Cases A and B.

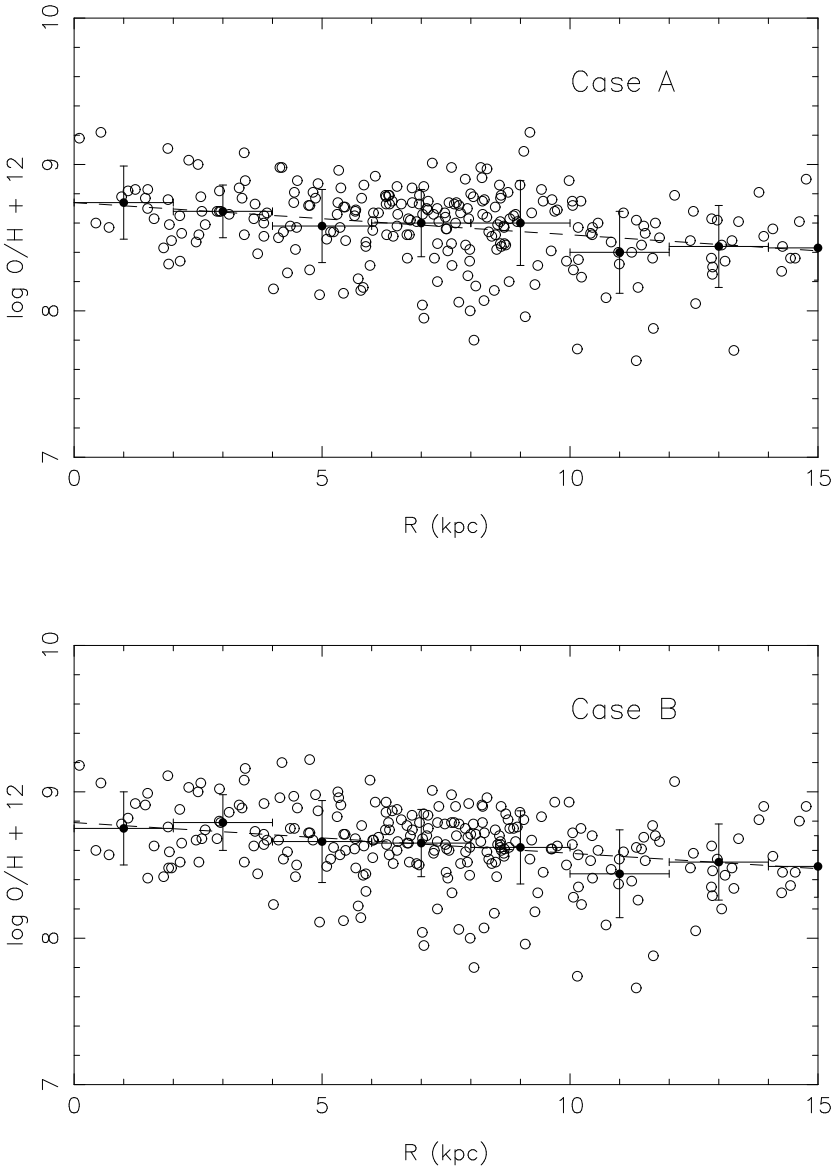

Fig. 3. The same as Figure 2, adopting average abundances in 2 kpc bins.

TABLE 1

COEFFICIENTS OF THE LINEAR FITS GIVEN BY EQUATION (1).

Case	A	σ_A	B	σ_B	r	σ_r
all data						
A	8.7625	0.0349	−0.0251	0.0041	−0.3565	0.2529
B	8.8146	0.0342	−0.0250	0.0040	−0.3626	0.2474
binned data						
A	8.7390	0.0316	−0.0223	0.0029	−0.9443	0.0487
B	8.7885	0.0344	−0.0213	0.0032	−0.9289	0.0532
disk + bulge nebulae						
A	8.6596	0.0265	−0.0156	0.0035	−0.2292	0.2731
B	8.6780	0.0266	−0.0124	0.0035	−0.1828	0.2743

considered a second order polynomial fit to the data, as defined in equation (2). The obtained coefficients are $C = 8.7581$, $D = -0.0238$, and $E = -0.0001$ for Case A, with $\chi = 0.0643$, and $C = 8.8364$, $D = -0.0312$, and $E = 0.0004$ with $\chi = 0.0614$ for Case B. In Case A the linear and quadratic fits are almost the same, and for Case B there is a slight difference between them for $R > 10\,\mathrm{kpc}$. Also, for Case A the gradients are essentially constant for the whole range of galactocentric distances, while for Case B some flattening is observed at large R. The gradient varies from $d(\mathrm{O/H})/dR \simeq -0.024$ to $-0.027\,\mathrm{dex/kpc}$ for Case A, with similar results for Case B.

Considering the total sample of disk objects, it can be seen that the average gradients found here are similar or somewhat flatter than previous determinations (see for example Maciel & Costa 2013). Since PN are relatively old objects, compared for example with HII regions, they may have been displaced from their original birthplaces. As a consequence, the measured gradients are probably flatter than before the displacement occurred. In other words, gradients derived from planetary nebulae are probably a lower limit to the original gradient. In fact, simulations with a large number of objects show that there is no way the gradients can be increased by the displacement of the progenitor stars. Additionally, most PN samples considered so far in the literature include objects of very different ages, as we have shown in our previous work on the age determination of the PN progenitor stars (Maciel et al. 2010, 2011, Maciel & Costa 2013), which also contributes to the flattening of the gradients.

Some recent chemodynamical models (see for example Chiappini et al. 2015, and references therein) suggest that the solar neighbourhood has been

contaminated with stars born at lower galactocentric distances, which are more metal-rich, since they come from a more metal-rich environment. As a result, a determination of the gradient on the basis of relatively old stars, such as the PN progenitor stars, lead to a flatter gradient. In fact, radial migration has been proposed as a common phenomenon in the Milky Way history, and models exploring this characteristic have been able to explain several chemical evolution constraints, such as the metallicity distribution and radial gradients (cf. Schönrich & Binney 2009).

4.2. *The Disk Sample divided into Height Groups*

The adopted groups were defined taking steps of 1,000 pc, 600 pc, 500 pc, 400 pc, and 200 pc, as follows: 2 groups ($\Delta = 1,000$ pc, 800 pc, and 600 pc); 3 groups ($\Delta = 500$ pc); 4 groups ($\Delta = 500$ pc); 6 groups ($\Delta = 400$ pc), and 11 groups ($\Delta = 200$ pc). A detailed description of the adopted groups is given in Table 2.

In view of the relatively small size of the sample considered, it is unlikely that a division into many groups would produce meaningful results, since the number of objects at each height would be small, so that we will focus on the division into 2 groups.

Let us consider first what is probably the most meaningful result, namely, the division into 2 groups, with steps of 1,000 pc, that is Group 1 has $|z| \leq 1,000$ pc and Group 2 has $|z| > 1,000$ pc. This limit gives an approximate separation of the thin disk and the thick disk. The main results are given in the first two rows of Table 3 (Case A), and in the plots shown in Figure 4. We can derive the following conclusions:

1. The intercept of Group 1 is higher than that of Group 2, meaning that the abundances of Group 1 are somewhat higher than those of Group 2, as expected if the former is younger than the latter. It can also be seen that Group 2 tends to have lower abundances than Group 1.

2. The gradient of Group 1 is slightly steeper than that of Group 2, but if the uncertainties are taken into account both gradients are essentially the same, that is, it is probably not possible to conclude that the objects at lower heights have different gradients from those at higher z values. Again, the correlation coefficients are small.

3. There are no evidences of any gradient inversion at low galactocentric distances. It should be mentioned that the samples considered so far do not include objects belonging to the galactic bulge (see section 4).

Considering now the remaining divisions into two groups, as given in the remaining rows of Table 3 and in Figures 5 and 6, it can be seen that conclusions 1 and 3 above are still valid, but there is some difference from conclusion 2 for the groups having $\Delta = 600$ pc, in the sense that the gradient of Group 2 is slightly steeper than that of Group 1. However, the difference is again small, so that conclusion 2 above is also valid for both groups.

The division into 3 groups is the same as in the previous case for $\Delta = 1,000$ pc, except that Group 1 is further subdivided into 2 groups. The results

TABLE 2

DEFINITION OF THE HEIGHT GROUPS.

Number of groups	Group	height (pc)
2	1	$\|z\| \leq 1,000$
	2	$\|z\| > 1,000$
2	1	$\|z\| \leq 800$
	2	$\|z\| > 800$
2	1	$\|z\| \leq 600$
	2	$\|z\| > 600$
3	1	$\|z\| \leq 500$
	2	$1000 \geq \|z\| > 500$
	3	$\|z\| > 1,000$
4	1	$\|z\| \leq 500$
	2	$1,000 \geq \|z\| > 500$
	3	$1,500 \geq \|z\| > 1,000$
	4	$\|z\| > 1,500$
6	1	$\|z\| \leq 400$
	2	$800 \geq \|z\| > 400$
	3	$1,200 \geq \|z\| > 800$
	4	$1,600 \geq \|z\| > 1,200$
	5	$2,000 \geq \|z\| > 1,600$
	6	$\|z\| > 2,000$
11	1	$\|z\| \leq 200$
	2	$400 \geq \|z\| > 200$
	3	$600 \geq \|z\| > 400$
	4	$800 \geq \|z\| > 600$
	5	$1,000 \geq \|z\| > 800$
	6	$1,200 \geq \|z\| > 1,000$
	7	$1,400 \geq \|z\| > 1,200$
	8	$1,600 \geq \|z\| > 1,400$
	9	$1,800 \geq \|z\| > 1,600$
	10	$2,000 \geq \|z\| > 1,800$
	11	$z > 2000$

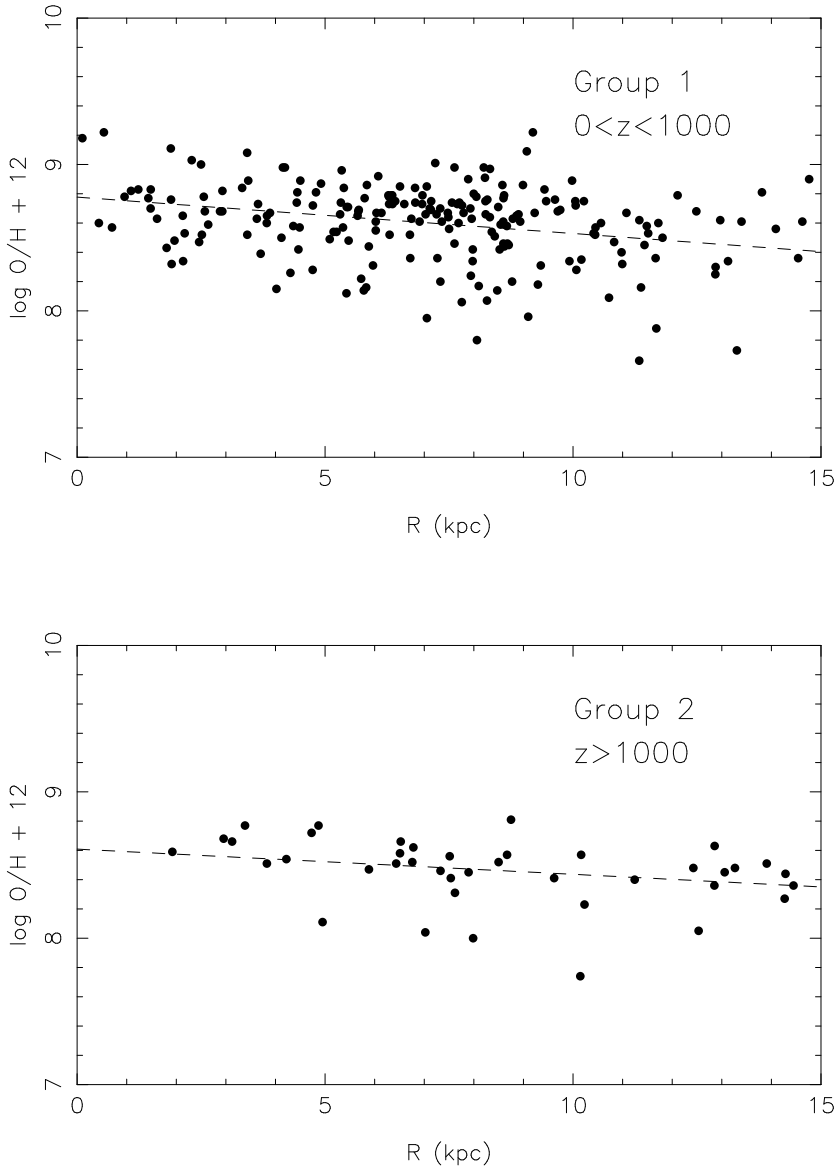

Fig. 4. The same as Figure 2, adopting 2 height groups with $\Delta = 1,000$ pc, Case A.

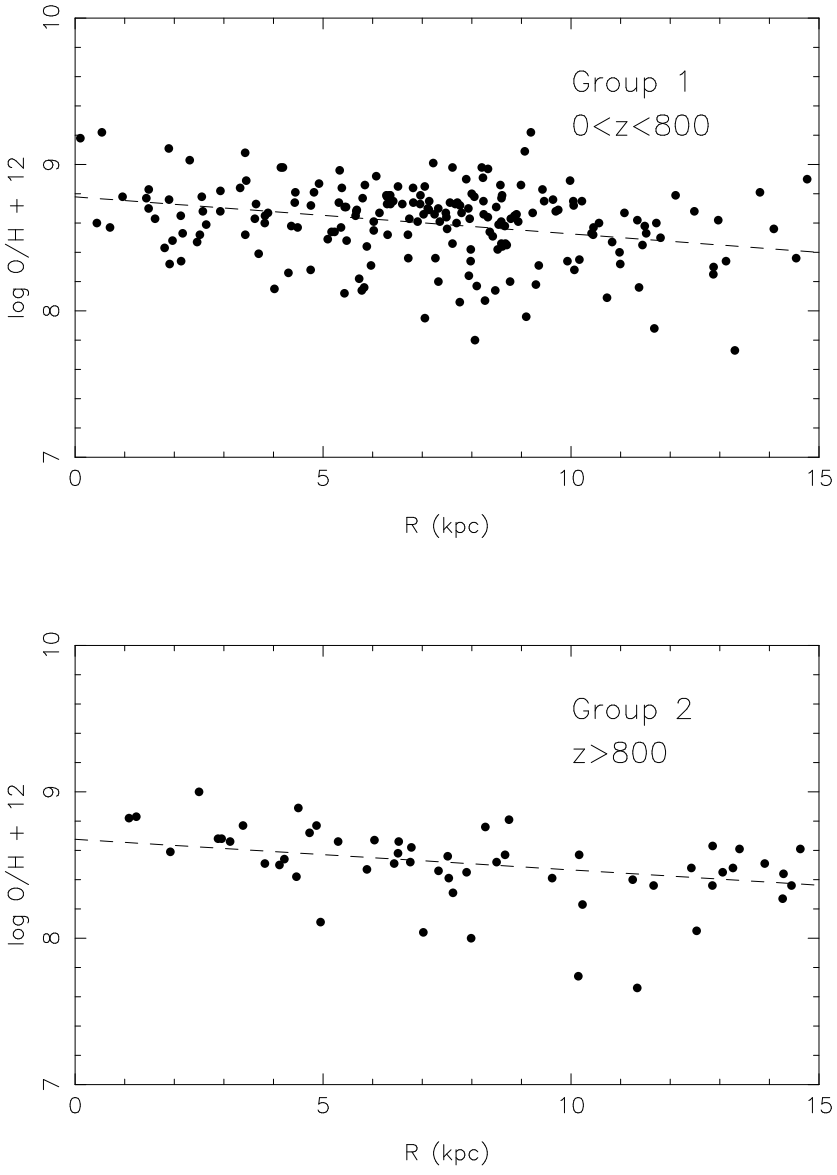

Fig. 5. The same as Figure 2, adopting 2 height groups with $\Delta = 800\,\mathrm{pc}$, Case A.

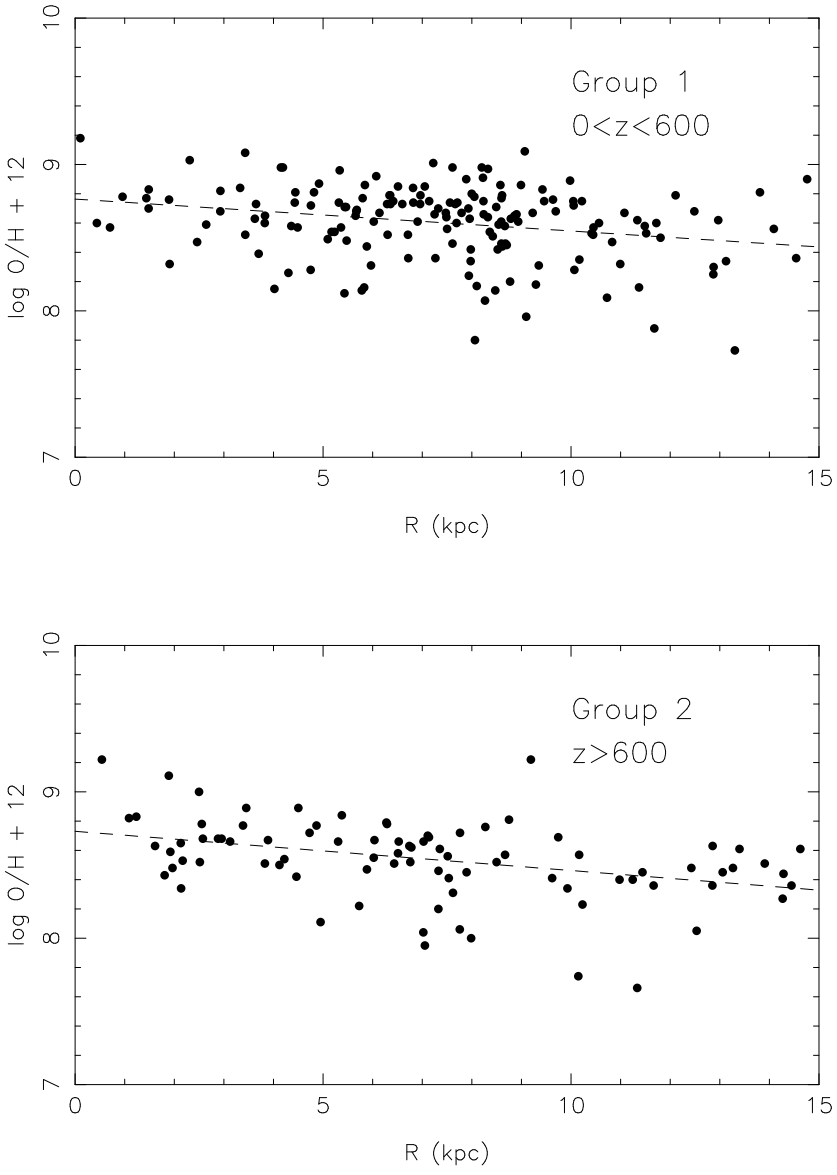

Fig. 6. The same as Figure 2, adopting 2 height groups with $\Delta = 600$ pc, Case A.

TABLE 3

COEFFICIENTS OF THE LINEAR FITS ADOPTING TWO HEIGHT GROUPS.

	A	σ_A	B	σ_B	r	σ_r
$\Delta = 1,000$ pc						
Group 1: $n = 218$	8.7773	0.0395	−0.0248	0.0048	−0.3300	0.2600
Group 2: $n = 45$	8.6086	0.0756	−0.0172	0.0073	−0.3400	0.2100
$\Delta = 800$ pc						
Group 1: $n = 202$	8.7790	0.0424	−0.0253	0.0053	−0.3200	0.2600
Group 2: $n = 61$	8.6755	0.0661	−0.0209	0.0065	−0.3900	0.2400
$\Delta = 600$ pc						
Group 1: $n = 168$	8.7639	0.0480	−0.0218	0.0059	−0.2800	0.2500
Group 2: $n = 95$	8.7302	0.0529	−0.0268	0.0057	−0.4400	0.2600

are similar, but clearly the new Group 2 has relatively few objects compared with the new Group 1. The division into 4 groups is also the same, except that both groups are further subdivided into 2 groups. The main difference from the previous results is that the new Group 3 has very few objects, thus showing no gradient at all. For the division into 6 groups we notice that Groups 4 and 5 have now very few objects, so that their gradient is meaningless. Otherwise, the results are similar as in the previous cases. For the division into 11 groups, Groups 6 to 10 have very few objects, so that their gradients are also meaningless. Otherwise, the results are similar as in the previous cases.

The results of section 4.1 are reinforced by the oxygen and neon gradients determined by Stanghellini and Haywood (2010), where different estimates for Peimbert Type I, II, and III objects have been made. This procedure implicitly assumes that the gradients are derived at different epochs, since Type I, II and III objects are expected to reflect increasing ages of the progenitor stars. It is found that the gradient is slightly flatter for type III nebulae, which are in principle located higher from the galactic disk, although the differences in the gradients are small and similar to those found in the present work. Comparing the results by SH with the present results for objects at different heights from the Galactic plane, it can be seen that our gradients at high $|z|$ are typically of -0.017 dex/kpc or slightly steeper, which is very similar to the Type III gradients derived by SH, namely -0.011 dex/kpc. For the objects closer to the disk, we have typically a gradient of -0.025 dex/kpc, while SH derives -0.035 dex/kpc for Type I nebulae, and for the intermediate mass population the corresponding gradients are about -0.021 dex/kpc, closer

to the SH values of -0.023 dex/kpc for Type II objects. Therefore, this is a confirmation that the Peimbert types as originally defined by Peimbert (1978) with a few posterior updates reflect the main population characteristics of the PN in the Galaxy.

4.3. *The Extended Sample: Disk, Bulge, and Interface Region*

The previous samples include essentially objects in the galactic disk, but there are many PN known to be in the galactic bulge or in the interface region. The distinction is not always clear, especially because of the uncertainties in the distances. Therefore, it is interesting to include these objects in our analysis, although some care must be taken to distinguish them from the previous samples of disk planetary nebulae.

Our own IAG sample includes 179 objects that in principle belong to the bulge population or to the interface between the bulge and the disk (see for example Cavichia et al. 2010, 2011, 2014, 2015). 94 objects from this sample have distances from Stanghellini et al. (2008). The abundances are from the IAG sample, as these objects are not included in the SH sample. Considering these objects, we have a total sample of $263 + 94 = 357$ nebulae.

The main results are shown in Figure 7, where the filled circles are data for the disk and the empty circles for the bulge/interface region. The latter extend to about $R = 6$ kpc, so that some of these objects are clearly not in the galactic centre. It can be seen that the inclusion of bulge/interface data slightly decreases the gradients compared with the average gradients measured in the outer disk, so that the trend observed for $R > 3 - 4$ kpc is somewhat modified. This effect should not be confused with a possible gradient inversion at large heights z from the plane, since the bulge/interface objects are located very close to the galactic plane. A similar distribution of bulge nebulae on the O/H $\times$ R plane was observed by Gutenkunst et al. (2008). It should be noted that there are some objects showing lower abundances ($\log$ O/H$+12 < 8$) than expected by the trend defined by most nebulae in both samples. It is possible that these objects can be explained by local abundance variations or by the fact that the corresponding central stars are older than most progenitor stars in the sample. Also, in this region the galactic bar may play an important role in the shaping of the gradient (cf. Cavichia et al. 2014).

The linear fits are also given in the last two rows of Table 1, again for Cases A and B. The slopes are still of the order of -0.02 dex/kpc, slightly lower than for the previous cases, but they are probably affected by the low abundance objects mentioned above. If we exclude the outliers, the gradients become closer to the disk sample. We can also obtain a polynomial fit to the data as in the previous case. The results are similar, and the gradients vary from a minimum of -0.014 dex/kpc to -0.037 dex/kpc for Case A, with similar results for Case B.

4.4. *Final Remarks*

Conclusions 1-3 listed in section 4.2 are in good agreement with our previous results on the time variation of the abundance gradient, as given in Maciel

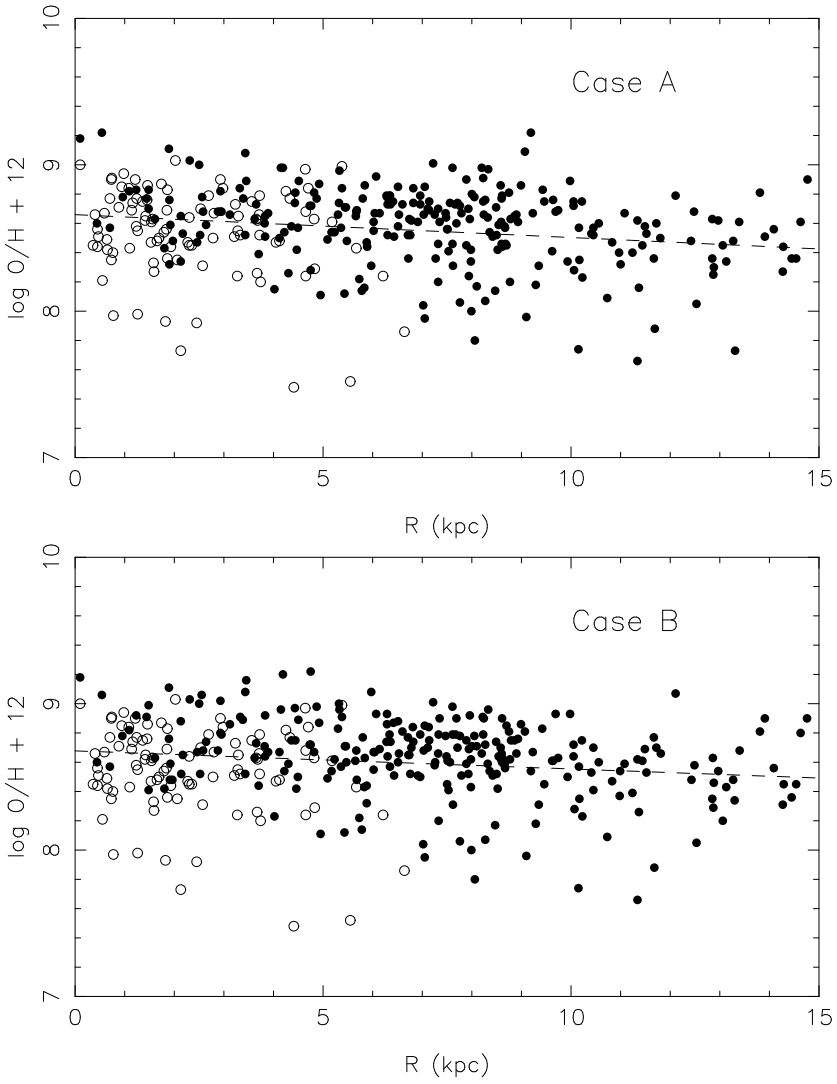

Fig. 7. The same as Figure 2, including objects from the bulge and interface region.

& Costa (2013). In particular, conclusion 1 states the observed differences in the average abundances of PN at high z (older objects) and low z (younger objects), and conclusion 2 states the similarity of the gradients of both groups. The first conclusion is consistent with the existence of a vertical abundance gradient, as found in thin and thick disk stars of the Milky Way on the basis of stellar data, as can be seen for example in Carrell et al. (2012) and Chen et al. (2011). Maciel & Costa (2013) have considered four samples of galactic PN for which the ages of their progenitor stars were estimated using three different methods. It was concluded that the younger objects have similar or somewhat higher oxygen abundances compared with the older objects, but the gradients are similar within the uncertainties. The actual magnitudes of the gradients are in the range -0.03 to -0.07 dex/kpc with an average of -0.05 dex/kpc, but depend on the adopted sample. The results of the present paper are closer to the lower limit, which is probably a consequence of the adopted distance scale and the effects of radial migration. Conclusion 2 is also supported by the results by Henry et al. (2010), who have separated their planetary nebula sample into two groups adopting the limit $z = 300$ pc. Again the slope of the group closer to the galactic plane is slightly steeper, but the distributions of the two subsamples are essentially the same.

Similar conclusions have been reached in our recent work on the abundance gradients as measured in symmetric and asymmetric PN (Maciel & Costa 2014). Since asymmetric PN, especially bipolars, are generally considered as younger than the symmetric objects, some difference in their gradients should probably be observed for sufficiently large samples. Considering the elements O, Ne, S, and Ar, it was concluded that the average abundances of the bipolar nebulae are somewhat higher than for non-bipolars for all elements studied, confirming our conclusion 1 above, but no important differences were found between the gradients, which are in the range -0.03 to -0.05 dex/kpc for oxygen. These results are also supported by some recent work by Pilkington et al. (2012) and Gibson et al. (2013), who concluded that there are no appreciable differences in the gradients in the local universe, near zero redshift, although steeper gradients are expected at much higher redshifts, beyond the age bracket considered in the present paper.

Cheng et al. (2012a, 2012b) have considered [Fe/H] abundances of a large sample of main sequence turnoff stars from the SEGUE survey in the region comprising galactocentric distances $6 < R(\mathrm{kpc}) < 16$ and heights $150 < |z|(\mathrm{pc}) < 1500$ relative to the galactic plane. They find that close to the disk ($|z| < 1500$ pc) the Fe gradient is about -0.06 dex/kpc, while for higher distances from the plane the gradient flatten out, with a negligible slope for $|z| > 1,000$ pc. Their sample is limited to objects with $R > 6$ kpc, so that no information is provided about a possible gradient inversion in the inner disk. Since the Fe gradient is probably slightly steeper than the oxygen gradient (see a discussion in Maciel et al. 2013), it can be concluded that their results are generally in agreement with our present results.

Acknowledgements. We are indebted to an anonymous referee for some

interesting comments and suggestions on a previous version of this paper. This work was partially supported by FAPESP and CNPq.

REFERENCES

Acker, A., Marcout, J., Ochsenbein, F., Stenholm, B. Tylenda, R. 1992, The Strasbourg-ESO catalogue of galactic planetary nebulae

Allende-Prieto, C., Beers, T. C., Wilhelm, R. et al. 2006, ApJ 636, 804

Boeche, C., Siebert, A., Piffl, T. et al. 2014, A&A 568, A71

Carrell, K., Chen, Y., Zhao, G. 2012, AJ 144, 185

Cavichia, O., Costa, R. D. D., Maciel, W. J. 2010, Rev. Mexicana Astron. Astrof. 46, 159

Cavichia, O., Costa, R. D. D., Maciel, W. J. 2011, Rev. Mexicana Astron. Astrof. 47, 49

Cavichia, O., Costa, R. D. D., Maciel, W. J. 2014, MNRAS 437, 3688

Cavichia, O., Costa, R. D. D., Maciel, W. J. 2015, In preparation

Chen, Y. Q., Zhao, G., Carrell, K., Zhao, J. K. 2011, AJ 142, 184

Cheng, J. Y., et al. 2012a, ApJ 746, 149

Cheng, J. Y., Rockosi, C. M., Morrison, H. L. 2012b, Galactic Archaeology: Near field cosmology and the formation of the Milky Way, ASP-CS 458, ed. W. Aoki et al.

Chiappini, C., Minchev, I., Anders, F., Brauer, D., Boeche, C., Martig, M. 2015, Proc. of the workshop Asteroseismology of stellar populations in the Milky Way, Astrophysics and Space Science Proceedings, Volume 39, eds. A. Miglio, L. Girardi, P. Eggenberger, J. Montalban, Springer, 111

Curir, A., Lattanzi, M. G., Spagna, A., Matteucci, F., Morante, G., Fiorentin, P. R., Spitoni, E. 2012, A&A 545, A133

Gibson, B. K., Pilkington, K., Bailin, J., Brook C. B., Stinson, G. S. 2013, Nuclei in the Cosmos XII, Proc. of Science, http://pos.sissa.it/archive/conferences/146/190/NIC

Gutenkunst, S., Bernard-Salas, J., Pottasch, S. R., Sloan, G. C., Houck, J. R. 2008, ApJ 680, 1206

Henry, R. B. C., Kwitter, K. B., Jaskot, A. E., Balick, B., Morrison, M. B., Milingo, J. B. 2010, ApJ 724, 748

Maciel, W. J., Costa, R. D. D. 2013, Rev. Mex. Astron. Astrof. 49, 333

Maciel, W. J., Costa, R. D. D. 2014, Asymmetrical planetary nebulae VI, Ed. C. Morisset, G. Delgado- Inglada, S. Torres-Peimbert http://www.astroscu.unam.mx/apn6/PROCEEDINGS/

Maciel, W. J., Costa, R. D. D., Idiart, T. E. P. 2010, A&A 512, A19

Maciel, W. J., Costa, R. D. D., Rodrigues, T. S. 2013, ESO Workshop, The Deaths of Stars and the Lives of Galaxies http://www.eso.org/sci/meetings/2013/DSLG/Presentations/S_I-Maciel.pdf

Maciel, W. J., Rodrigues, T. S., Costa, R. D. D. 2011, Rev. Mex. Astron. Astrof. 47, 401

Minchev, I., Chiappini, C., Martig, M. 2014, A&A 572, A92

Nordström, B., Mayor, M., Andersen, J. et al. 2004, A&A 418, 989

Peimbert, M., 1978, IAU Symp. 76, Ed. Y. Terzian (Dordrecht: Reidel), 215

Pilkington, K., Few, C. G., Gibson, B. K., Calura, F. et al. 2012, A&A, 540, A56

Sancho Miranda, M. Pilkington, K., Gibson, B. K., et al. 2014, Nuclei in the Cosmos XIII, poster 22

Schönrich, R., Binney, J. 2009, MNRAS 399, 1145
Spitoni, E., Matteucci, F. 2011, A&A 531, A72
Stanghellini, L., Haywood, M. 2010, ApJ 714, 1096
Stanghellini, L., Shaw, R. A., Villaver, E. 2008, ApJ 689, 194

W. J. Maciel, and R. D. D. Costa: Instituto de Astronomia, Geofísica e Ciências Atmosféricas, Universidade de São Paulo - Rua do Matão 1226, CEP 05508-090, São Paulo SP, Brazil (wjmaciel@iag.usp.br, roberto.costa@iag.usp.br.)

O. Cavichia: Instituto de Física e Química, Universidade Federal de Itajubá, Av. BPS 1303, Pinheirinho, CEP 37500-903, Itajubá, MG, Brazil (cavichia@unifei.edu.br.)